REDVET - Revista electrónica de Veterinaria - ISSN 1695-7504
Vol 25, No. 2 (2024)
http://www.veterinaria.org
Article Received: Revised: Accepted:

Structural, Spectroscopic, *In Silico*, And *In Vitro* Studies On 4-Amino-5-Chloro-2,6-Dimethylpyrimidine: A Potential Antimicrobial And Lung Cancer Drug

T. Ancy[1], M.R.Meera[2]*, C.Vijayakumar[3], R. Premkumar[4],

[1]Research scholar (Reg.No.20223232132004), Department of Physics, St. Jude's College, Thoothoor-629 176, Affiliated to Manonmanium Sundaranar University, Abishekapatti, Tirunelveli-627 012, Tamil Nadu, India.
[2*]Department of Physics, Sree Ayyappa College for Women, Chunkankadai, Nagercoil-629 003, Tamil Nadu, India.
[3]Department of Physics, St. Jude's College, Thoothoor, Kanyakumari District-629176, Tamil Nadu, India.
[4] M.Sc., Ph. D., Assistant Professor Advanced Materials Research Centre (AMRC), PG and Research Department of Physics, N.M.S.S.V.N. College, Madurai-625 019, Tamil Nadu, India. TEL: +91-9080067494, E-mail: rjpremphy@gmail.com

***Corresponding Author:** Dr. M.R. Meera, Ph. D.,
*Associate Professor and Head, Department of Physics, Sree Ayyappa College for Women, Chunkankadai, Nagercoil 629 003, Tamil Nadu, India. TEL: +91-9443692523, E-mail: meeranairmrm17@gmail.com

Abstract
This study investigates the structural, vibrational, electronic, and biological properties of 4-Amino-5-chloro-2,6-dimethylpyrimidine (ACDMP), with a focus on its potential as a lung cancer drug. Using density functional theory (DFT) with the B3LYP functional and the 6-311G++ (d,p) basis set, the molecular structure of ACDMP was optimized and calculated its vibrational frequencies. Experimental Fourier Transform Infrared (FT-IR) and Raman spectra were recorded, and theoretical values were scaled for comparison, showing good agreement. UV-Vis spectral analysis indicated significant intramolecular charge transfer. Frontier molecular orbitals (FMOs) analysis revealed a HOMO-LUMO gap of 4.71 eV, suggesting high reactivity and potential bioactivity. Mulliken atomic charge distribution supports the delocalization of charges, which contributes to the bioactivity of ACDMP. The compound also exhibited notable antibacterial activity against *Staphylococcus aureus*. Additionally, *in vitro* cytotoxicity assays on A549 human lung cancer cells and HeLa cervical cancer cells showed that ACDMP is more effective against lung cancer cells. Moreover, the molecular docking studies demonstrated that ACDMP acts as a potent inhibitor of dipeptidyl peptidase-IV, a key enzyme in lung cancer. These findings highlight ACDMP's potential as an effective agent in lung cancer treatment.

Keywords: 4-Amino-5-chloro-2,6-dimethylpyrimidine; Density Functional Theory; Antibacterial Activity; In Vitro Cytotoxicity; Molecular Docking; Lung Cancer Therapeutics

1. Introduction

Pyrimidine derivatives possess significant medicinal properties and are crucial in drug design due to their extensive pharmacological activity, combined with relatively low side effects and toxicity. They are characterized by high bioavailability, minimal drug resistance, broad-spectrum efficacy, and enhanced therapeutic effects [1]. Additionally, their exceptional physical, thermal, optical, and biological properties make them valuable for use as fabric dyes, fluorophores, and optical brightening agents. Bioactive pyrimidine compounds have proven useful as antioxidants, anticoagulants, antivirals, antimicrobials, antiparasitics, antifungals, anti-diabetics, anticancer agents, anti-neurodegenerative agents, analgesics, and anti-inflammatory agents [2-7]. The pyrimidine ring, with its extensive conjugated system and charge-transport properties, is electron-rich, which facilitates interactions with ions and molecules. Fluorescent probes, biological stains, and ion receptors based on pyrimidine are increasingly important in monitoring complex biological processes, enzyme activity, and precise pharmacological and pharmacokinetic characteristics in living cells [8-13].

Numerous reviews in the literature have highlighted the advanced applications of pyrimidines, particularly emphasizing their anticancer and antioxidant properties [14-19]. Notably, several pyrimidine-based compounds and metal complexes exhibit antiviral, antioxidant, antimicrobial, anti-HIV, and anticoagulant properties. Synthetic aminopyrimidine-based drugs, such as warfarin and acenocoumarol, which are vitamin K antagonists, are commonly used for treating blood coagulation disorders [20-25]. These wide-ranging applications of aminopyrimidines have inspired the theoretical and experimental investigations of the molecule 4-Amino-5-chloro-2,6-dimethylpyrimidine (ACDMP). Such studies could lead to the development of new molecules with diverse bio-medicinal properties.

In this study, the structural, vibrational and electronic excited state characteristics of ACDMP, which relate to its stability and reactivity, were examined theoretically using the density functional theory (DFT) method. DFT is a valuable technique for calculating vibrational frequencies, molecular geometries, and molecular orbital energies. Moreover, the B3LYP functional has been shown to offer an excellent balance between vibrational spectral accuracy and computational efficiency for medium to large molecules [26-28]. *In vitro* cytotoxicity analysis is a widely used

screening test in biological evaluation, helping to assess cell growth, morphological effects, and reproduction influenced by medical devices [29]. Molecular docking has been extensively used in drug development to explore potential protein-ligand interactions [30].

A review of the literature revealed that no DFT quantum chemical computational studies on ACDMP have been conducted to date. In this work, the structure of ACDMP was initially optimized using the Gaussian 09 program [31]. The vibrational spectra (FT-Raman and FTIR) were recorded and simulated for the molecule. The kinetic stability and reactivity of ACDMP were determined through frontier molecular orbitals analysis. The electronic absorption data in aqueous solution were presented and compared experimentally for structural identification. The Mulliken charge distribution was also calculated. The *in vitro* antibacterial and anticancer studies of the title compound were also carried out. Additionally, docking analysis was carried out to assess the inhibitory potential of ACDMP against two different cancer-related proteins.

2. Materials and Methods

2.1 Experimental characterizations

The ACDMP compound, with 99% purity, was sourced from Sigma-Aldrich, Chemicals Co., St. Louis, MO, USA. The Fourier transform-infrared (FT-IR) spectrum was recorded using a Perkin Elmer Spectrum 1 FT-IR spectrometer, employing the KBr pellet method at room temperature with a resolution of 1.0 cm^{-1}. The FT-Raman spectrum was recorded using a BRUKER RFS 27: Stand-alone Raman spectrometer at room temperature with a resolution of 2 cm^{-1}. Both the FT-IR and FT-Raman spectra were obtained in the wavenumber range of 3500-400 cm^{-1}. The UV-Vis spectrum was measured using a Shimadzu UV-3600 UV Vis-NIR spectrophotometer (Shimadzu Scientific Instruments, Columbia, MD) over the wavelength range of 200-600 nm, with ethanol as the solvent. Additionally, antibacterial activity was tested against four different bacterial strains: *Staphylococcus aureus, Klebsiella pneumoniae, Escherichia coli*, and *Pseudomonas aeruginosa*. The MTT assay was performed to evaluate the anticancer efficacy of the ACDMP molecule against A549 human lung cancer cell lines and HeLa human cervical cancer cell lines.

2.2 Computational details

The molecular structure of the ACDMP molecule was optimized using the DFT/B3LYP method with a 6-311G++ (d,p) basis set via the Gaussian 09 program [32,33]. The most stable structure of the molecule was identified through this DFT/B3LYP method, also employing the 6-311G++ (d,p) basis set. Vibrational wavenumbers were then calculated for this optimized structure. The calculated vibrational wavenumbers were assigned based on potential energy distribution (PED) analysis, performed using the VEDA 4.0 program [34]. The UV-Vis spectrum was simulated using the time-dependent (TD)-DFT/B3LYP method, incorporating the polarizable continuum model (PCM) and utilizing the 6-311G++ (d,p) basis set with ethanol as the solvent. The optimized molecular structure, along with the calculated vibrational wavenumbers, UV-Vis spectrum, Mulliken atomic charge distribution, molecular electrostatic potential (MEP) surface, and frontier molecular orbitals (FMOs), were visualized using the GaussView 05 [35] program. All calculations were performed at the ground state energy level of the ACDMP molecule, without imposing any constraints on the potential energy surface. Additionally, molecular docking analysis was performed using AUTODOCK 4.0.1 software to investigate the inhibitory potential of the ACDMP molecule against targeted proteins associated with lung and cervical cancers.

3 Results and discussion

3.1 Molecular geometry and symmetry

The structure of the ACDMP molecule was optimized by the DFT/B3LYP level of theory using the cc-pVTZ basis set. The optimized structure of ACDMP is shown in Fig. 1. The least energy value of ACDMP is calculated to be −647.71 a.u., which confirms that the molecule is a true minimum energy on the potential energy surface [36]. Moreover, the molecular geometry of the ACDMP molecule possesses C_1 point symmetry. The title molecule has 18 atoms and 48 normal modes of vibration, which all belongs to the similar type of symmetry species (A). All modes are found to be Raman and infrared active, which confirms the non-centro symmetry structure of ACDMP molecule.

Table 1 provides the optimized structural parameters of the ACDMP molecule, calculated using DFT/B3LYP with the cc-pVTZ basis set. The table includes bond lengths, bond angles, and dihedral angles, which are crucial for understanding the geometric configuration and stability of the molecule. The bond lengths of the ACDMP molecule range from 0.9858 Å to 1.5251 Å, with significant bond lengths including N1-C2 (1.3294 Å), N1-C14 (1.3705 Å), C2-C3 (1.4178 Å), C3-C4 (1.3762 Å), C4-C13 (1.4262 Å), C5-C6 (1.4452 Å), and C6-O9 (1.3755 Å). These values indicate the strength and type of bonding interactions present in the molecule. The bond angles in the molecule range from 104.25° to 123.82°, with noteworthy angles including C2-N1-C14 (118.32°), N1-C2-C3 (122.58°), C2-C3-C4 (119.42°), C4-C13-C5 (123.82°), and C6-O9-C15 (119.56°). These angles provide insight into the molecular geometry, suggesting that the molecule adopts a non-linear, complex three-dimensional structure, which can influence its reactivity and interactions with other molecules. The dihedral angles provide information about the spatial arrangement of atoms within the molecule. The key dihedral angles include C14-N1-C2-C3 (0.15°), N1-C2-C3-C4 (0.01°), and C2-C3-C4-H18 (0.16°). These small values indicate minimal torsion in these parts of the molecule, suggesting a relatively

REDVET - Revista electrónica de Veterinaria - ISSN 1695-7504
Vol 25, No. 2 (2024)
http://www.veterinaria.org
Article Received: Revised: Accepted:

planar configuration in those regions. Thus, the bond lengths and angles suggest a stable configuration of the ACDMP molecule, while the dihedral angles indicate the specific spatial orientation of atoms, which is essential for understanding the molecule's physical and chemical properties. The structural analysis evidences the reactivity of the title molecule.

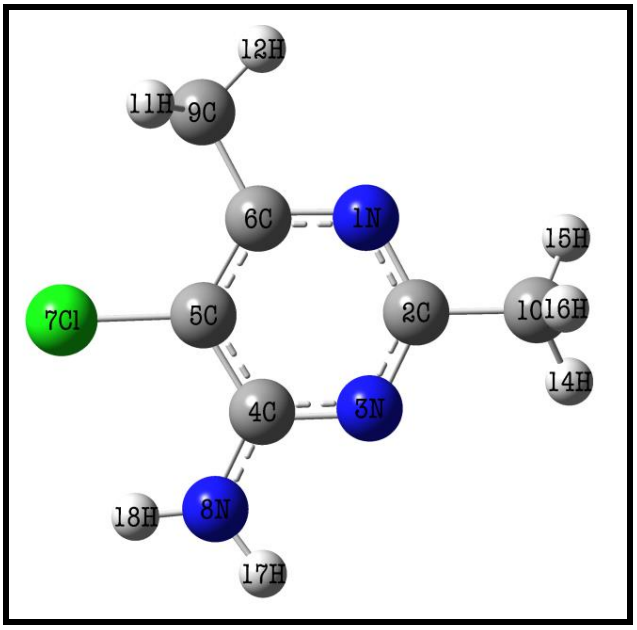

Fig.1. The optimized molecular structure of ACDMP molecule.

Table 1. The optimized structural parameters of the ACDMP molecule calculated by the DFT/B3LYP method with cc-pVTZ basis set.

Structural Parameters	cc-pVTZ	Structural Parameters	cc-pVTZ	Structural Parameters	cc-pVTZ
Bond length (Å)		**Bond angle (degree)**		C2-C3-C4-C13	0.03
N1-C2	1.3294	C2-N1-C14	118.32	H12-C3-C4-C13	0.02
N1-C14	1.3705	N1-C2-C3	122.58	H17-C3-C4-C14	0.05
C2-C3	1.4178	N1-C2-H16	117.28	C2-C3-C4-C14	0.13
C2-H16	1.0852	C3-C2-H16	120.05	C2-C3-C4-H18	0.15
C3-C4	1.3762	C2-C3-C4	119.42	H16-C2-C3-H17	0.12
C3-H17	1.0825	C2-C3-H17	119.39	H16-C2-C3-C4	0.14
C4-H18	1.0835	C4-C3-H17	121.02	C3-C2-C6-C5	0.16
C4-C13	1.4262	C3-C4-H18	120.85	C3-C2-C6-C7	0.05
C5-C1	1.3855	C3-C4-C14	119.14	H16-C2-C6-C7	0.03
C5-H19	1.0822	H12-C4-C13	119.15	H16-C2-C6-O9	0.01
C5-C6	1.4452	C6-C5-H19	118.65	N1-C2-C6-C5	0.04
C6-C7	1.4155	C6-C5-C13	120.14	N1-C2-C6-C7	0.02
C6-O9	1.3755	H13-C5-C13	121.10	C3-C2-C6-O9	0.01
C7-C8	1.3758	C5-C6-C7	120.15	C2-C6-C7-C8	0.01
C7-H20	1.0758	C5-C6-O9	116.39	C2-C6-C7-H20	0.04
C8-C14	1.4223	C7-C6-O9	123.39	C2-C6-C7-C14	0.12
C8-N12	1.4255	C6-C7-C8	120.05	H19-C6-C7-H20	0.06
O9-C15	1.5251	C6-C7-H20	120.16	H19-C6-C7-C14	0.03
C15-H21	1.0823	C8-C7-H20	119.58	H19-C6-C7-C8	0.01
C15-H22	1.0823	C7-C8-C14	120.10	C2-C6-C7-H20	0.02
C15-H23	1.0868	C7-C8-N12	122.49	C6-C7-C8-N12	0.11
N12-O10	1.2452	C14-C8-N12	116.89	C6-C7-C8-C14	0.15
N12-O11	1.2353	C6-O9-C15	119.56	C2-C6-C7-C8	0.03
O24-H40	0.9858	C4-C13-C5	123.82	H20-C7-C8-N12	0.01
O24-C34	1.4325	C4-C13-C14	116.48	H20-C7-C8-C14	0.02
C34-C36	1.3835	C5-C13-C14	119.85	C2-C6-C7-C8	0.13
C34-C36	1.4428	N1-C14-C8	117.82	C7-C8-N12-C4	0.01
C36-H39	1.0845	N1-C14-C13	123.32	C6-C7-C8-N12	0.03
C36-C35	1.4348	C8-C14-C13	118.85	C6-C7-C8-C14	0.05
C35-H38	1.0835	O9-C15-H21	104.25	C8-N12-O10-H21	0.02

C35-C32	1.3858	O9-C15-H22	111.57	C8-N12-O10-H22	0.14
C32-C33	1.4428	O9-C15-H23	111.25	N12-O10-H21-H22	0.01
C33-H37	1.0845	C8-N12-O10	120.10	N12-O10-H21-C14	0.03
C33-C31	1.3747	C8-N12-O11	122.01	C6-C7-C8-N12	0.11
C31-N29	1.4245	O10-N12-O11	118.25	H20-C7-C8-C14	0.02
N29-O25	1.2542	**Dihedral angle (degree)**			
N29-O26	1.2458	C14-N1-C2-C3	0.15		
C32-N30	1.4256	N1-C2-C3-C4	0.01		
N30-O27	1.2547	C2-C3-C4-H18	0.16		

3.2 Vibrational spectral analysis

The experimentally observed and theoretically simulated infrared spectra of the ACDMP molecule are shown in Fig. 2. Similarly, the observed and simulated Raman spectra of the ACDMP molecule are shown in Fig. 3. In order to account for the anharmonicity in DFT results, the vibrational calculated frequencies were scaled by scaling factors using the formula [37],

$C = \Sigma(\nu_i * \omega_i)/\Sigma\omega_i^2$

where ν_i and ω_i are experimental and theoretical frequencies, respectively and C is the scaling factor. The scaling factors for stretching and bending modes of ACDMP molecule are calculated as 0.9700 and 0.9971, respectively. The vibrational frequencies, IR intensity, and Raman scattering activity and the corresponding vibrational assignments of ACDMP molecule were listed in Table 2. The calculated vibrational frequencies values were correlated well with the experimental values.

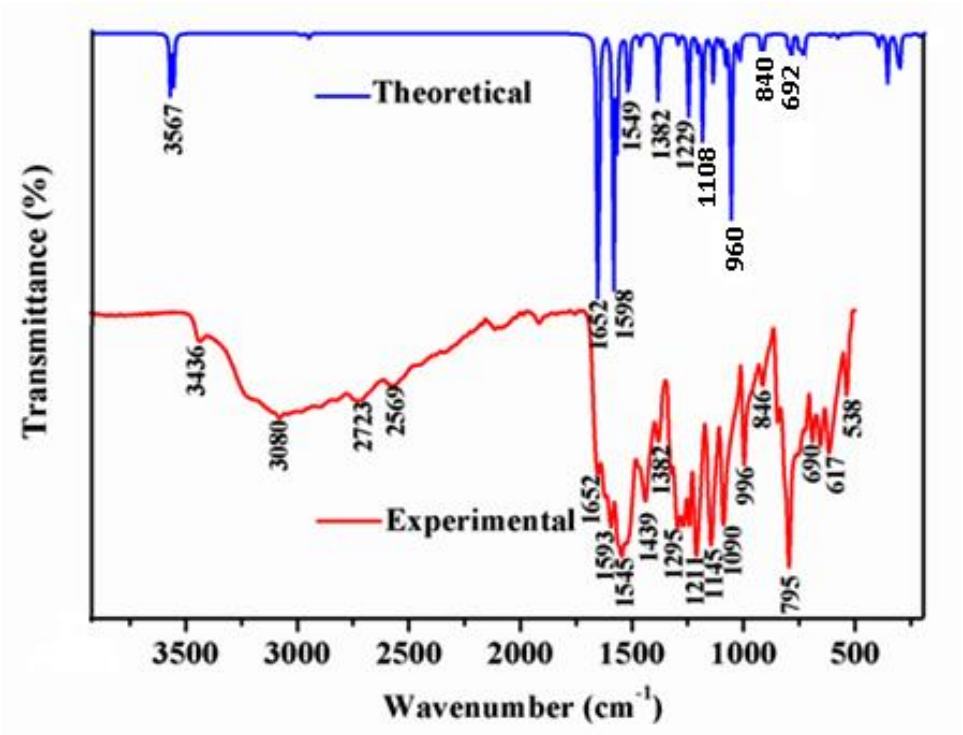

Fig. 2. The infrared spectra of ACDMP molecule.

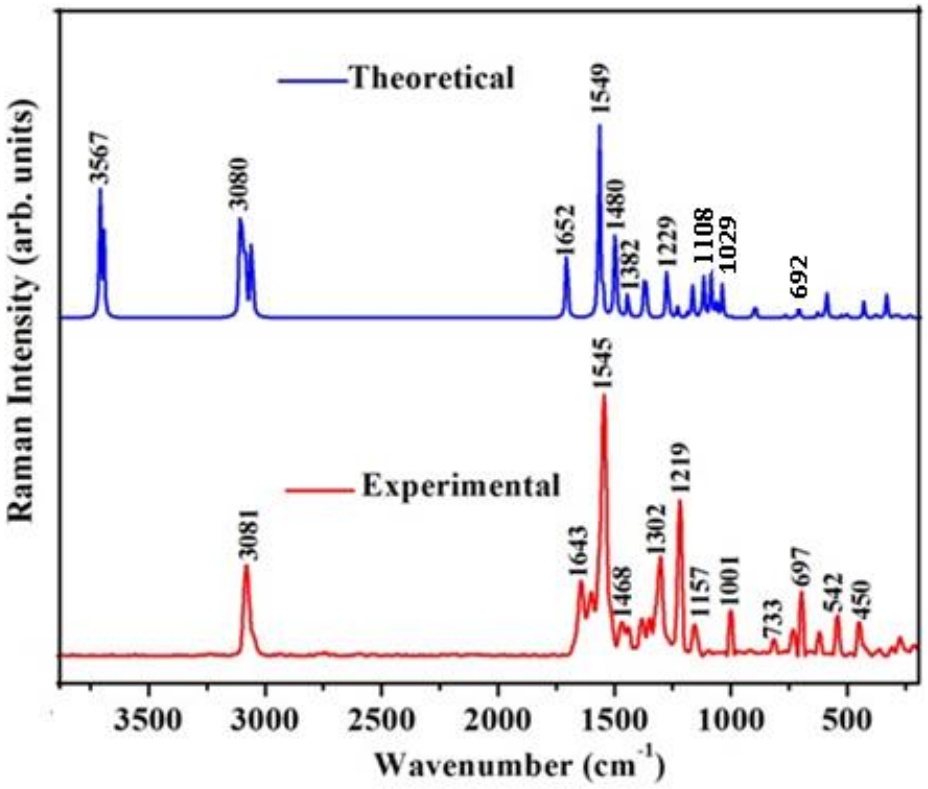

Fig. 3. The Raman spectra of the ACDMP molecule.

3.2.1 CH_3 Vibrations

In the ACDMP molecule, both symmetric stretching (νs C-H_3) and asymmetric stretching (ν_{as} C-H_3) modes are predicted to be prominent. Specifically, the asymmetric stretching of the CH_3 group was calculated to occur at 3080, 3073, 3023, and 3021 cm^{-1}, while the symmetric stretching modes are predicted at 2974 and 2971 cm^{-1}. The in-plane bending vibrations of CH_3 were computed to fall within the range of 1549 to 1498 cm^{-1}, with a strong peak observed at 1545 cm^{-1} in both the FT-IR and FT-Raman spectra. Additionally, the CH_3 torsional vibrations are predicted to appear in the lower vibrational range. These theoretical predictions align well with the experimental literature, indicating a strong agreement between the computed and observed values [38-40].

3.2.2 N-H_2 Vibrations

The stretching vibrations of N-H_2 are prominent in the spectrum. Specifically, the N-H_2 asymmetric stretching vibration of the molecule was calculated at 3567 cm^{-1}. For N-H_2 symmetric stretching, the calculated frequency is 3080 cm^{-1}, with a weak band observed at 3080 cm^{-1} in the FT-IR spectrum and a very strong peak at 3081 cm^{-1} in the FT-Raman spectrum. The in-plane bending vibrations of N-H_2 were calculated at 1652 cm^{-1} and 1243 cm^{-1}, with corresponding medium peaks observed at 1652 cm^{-1} and 1211 cm^{-1} in the FT-IR spectrum, and strong peaks at 1643 cm^{-1} and 1219 cm^{-1} in the FT-Raman spectrum. Additionally, the N-H_2 out-of-plane bending vibration was calculated at 560 cm^{-1}, with medium peaks observed at 538 cm^{-1} the FT-IR spectrum and 542 cm^{-1} in the FT-Raman spectrum [40-42].

3.2.3 CCl Vibrations

The C-Cl stretching vibration was calculated at 1029 cm^{-1}, with the corresponding peak observed as a strong peak at 996 cm^{-1} in the FT-IR spectrum and a medium peak at 1001 cm^{-1} in the FT-Raman spectrum [42-45].

3.2.4 Pyrimidine Ring Vibrations

The C-C stretching combined with C-N stretching in the pyrimidine ring was calculated at 1598 cm^{-1}, with the corresponding experimental peak observed as a medium peak at 1593 cm^{-1}. Additionally, this vibrational mode was calculated at 1480 and 1382 cm^{-1}, while experimental peaks were observed at 1468 and 1302 cm^{-1}. The torsional vibration of the pyrimidine ring (τ Ring) was calculated at 639 and 603 cm^{-1} [42-45].

The comparison between experimental and scaled frequencies shows a strong correlation, with discrepancies generally within a reasonable range. This confirms the reliability of the vibrational assignments and validates the computational methods used.

REDVET - Revista electrónica de Veterinaria - ISSN 1695-7504
Vol 25, No. 2 (2024)
http://www.veterinaria.org
Article Received: Revised: Accepted:

Table 2. The calculated vibrational frequencies (cm^{-1}), IR intensities (Km mol^{-1}), Raman scattering activity ($Å^4$ amu^{-1}), reduced mass (amu), force constants (mDyne/$Å^{-1}$) and vibrational assignments based on PED calculations for the ACDMP molecule.

S. No.	Observed Wavenumber (cm^{-1})		Wavenumber (cm^{-1})		IR Intensity (Km mol^{-1})	Raman scattering activity ($Å^4$ amu^{-1})	Reduced Mass (amu)	Force Constant (mDyne/ $Å^{-1}$)	Assignment with PED (%)
	FT-IR	FT-Raman	Calculated	Scaled					
1			3675	3567	0.5911	9.2260	1.2265	0.0045	ν_{as} N-H_2 (99%)
2	3436w		3547	3441	0.3565	5.8177	1.1791	0.0036	ν_s N-H_2 (99%)
3	3080w	3081vs	3175	3080	6.9738	10.4301	1.2256	0.0048	ν_{as} C-H_3 (98%)
4			3168	3073	2.5780	11.8722	1.2279	0.0049	ν_{as} C-H_3 (98%)
5			3116	3023	4.6062	12.6463	1.2105	0.0042	ν_{as} C-H_3 (99%)
6			3114	3021	1.2547	10.1189	1.2071	0.0039	ν_{as} C-H_3 (99%)
7			3066	2974	6.9827	20.2549	1.1927	0.0031	ν_s C-H_3 (97%)
8			3063	2971	18.7869	12.7874	1.0522	0.0026	ν_s C-H_3 (96%)
9	1652m	1643s	1672	1652	163.2347	3.5642	4.6730	7.8941	β N-H_2 (90%)
10	1593m		1602	1598	211.7616	7.2059	4.2750	6.4647	β N-H_2 (37%), νϕC-C (45%), νϕC-N (10%)
11	1545s	1545vs	1551	1549	9.6910	12.9628	1.3884	1.9695	β C-H_3 (46%)
12			1550	1545	13.2970	27.8279	1.0431	1.4782	β C-H_3 (45%)
13			1549	1544	4.3259	18.3130	1.0437	1.4764	β C-H_3 (48%)
14			1542	1538	51.8382	25.5978	1.1321	1.5868	β C-H_3 (43%)
15			1502	1498	14.3858	1.8936	2.8951	3.8492	β C-H_3 (43%)
16		1468	1484	1480	57.2853	1.0667	4.3123	5.5987	β N-H_2 (12%), νϕC-C (53%), νϕC-N (13%)

Table 2 (Continued)

S. No.	Observed Wavenumber (cm^{-1})		Wavenumber (cm^{-1})		IR Intensity (Km mol^{-1})	Raman scattering activity ($Å^4$ amu^{-1})	Reduced Mass (amu)	Force Constant (mDyne/ $Å^{-1}$)	Assignment with PED (%)
	FT-IR	FT-Raman	Calculated	Scaled					
17	1439m		1454	1450	16.4219	16.3465	1.2449	1.5510	ν_s C-H_3 (92%)
18	1382w		1448	1443	20.3523	19.0566	1.2145	1.5019	ν_s C-H_3 (91%)
19		1302s	1410	1382	138.9347	6.7634	7.0459	8.2610	β N-H_2 (15%), νϕC-C (66%), νϕC-N (12%)
20	1295m		1362	1358	43.2939	10.4963	5.6123	6.1348	β C-H_3 (24%), νϕC-N (13%)
21	1211s	1219vs	1243	1229	33.8939	4.0508	3.4281	3.1253	β C-H_3 (13%), νϕC-N (16%)
22			1121	1118	5.4633	1.8681	2.4566	1.8197	β C-H_3 (14%), β N-H_2 (16%), νϕC-C (16%)
23	1145vs	1157w	1111	1108	18.6408	0.7137	2.6871	1.9553	β C-H_3 (19%), β N-H_2 (18%),
24			1109	1106	1.0707	0.5444	1.5850	1.1491	β C-H_3 (38%),
25	1090vs		1096	1093	14.8189	0.3109	1.5727	1.1133	β C-H_3 (43%),
26			1071	1068	36.4934	2.5343	1.8437	1.2462	β C-H_3 (45%), β N-H_2 (12%),
27	996s	1001m	1032	1029	65.4020	5.0528	5.7585	3.6170	ν C-Cl (56%)
28			963	960	20.1007	2.4322	2.5959	1.4212	β C-H_3 (24%), νϕC-N (13%)
29	846w		937	934	1.7105	4.6188	4.2523	2.2031	β N-H_2 (32%),
30	795vs	733w	842	840	45.5087	0.6304	7.6722	3.2073	β CCN (23%), β NCN (12%), β HCH (10%)
31	690w	697s	694	692	12.6219	0.1523	4.5593	1.2954	β HCH (14%)
32			641	639	0.2581	0.1324	5.0129	1.2152	τ Ring
33			605	603	23.2640	2.2583	3.2037	0.6926	η N-H_2 (22%)
34			605	603	4.8827	23.9864	5.6613	1.2228	τ Ring
35	538m	542m	562	560	30.6218	2.0023	1.1627	0.2168	η N-H_2 (21%)

Table 2 (Continued)

S. No	Observed Wavenumber (cm^{-1})	Wavenumber (cm^{-1})	IR Intensity	Raman scattering	Reduced Mass	Force Constant	Assignment with PED (%)

·	FT-IR	FT-Raman	Calculated	Scaled	(Km mol^{-1})	activity ($Å^4$ amu^{-1})	(amu)	(mDyne/ $Å^{-1}$)	
36			553	551	7.8677	5.2449	6.8440	1.2349	β CCNH (23%)
37			526	524	1.9464	0.0296	2.8754	0.4691	β ClCCC (12%), CCCN (13%)
38		450m	496	495	243.0557	0.4614	1.1971	0.1741	η N-H_2 (18%)
39			388	387	3.9075	15.3563	6.2596	0.5559	β CNCC (13%), β NCNC (11%)
40			321	320	0.0037	0.6494	5.8172	0.3539	β ClCCN (14%), β CNCN (18%)
41			304	303	11.3577	1.9061	3.3406	0.1828	β CNCN (20%)
42			280	279	2.5948	1.0901	2.6791	0.1242	β CNCC (25%)
43			234	233	1.5156	0.2551	6.1668	0.1997	β CCNC (12%)
44			220	219	1.9680	1.1999	6.6755	0.1911	β CCCCl (15%)
45			190	186	9.3887	0.9131	3.1761	0.0679	β CCNC (17%)
46			104	103	0.8621	0.2042	1.0759	0.0069	τ CH_3 (21%)
47			90	89	0.5162	0.1120	3.7706	0.0181	τ CH_3 (26%)
48			38	38	0.6626	0.3380	1.0399	0.0009	τ CH_3 (32%)

w-weak, m-medium, s-strong, vs-very strong ν - stretching; ν_s - symmetric stretching, ν_{as} - asymmetric stretching β - in-plane bending, η - out of plane bending, τ-torsion, ϕ - pyrimidine ring

3.3 UV-Visible analysis

UV-Visible spectral examination was carried out, both theoretically and experimentally, to investigate the electronic behavior of ACDMP [46]. The observed and simulated UV-Visible spectrum of the ACDMP molecule is shown in Fig. 4. The electronic transition parameters such as excitation energy (E), excitation wavelength (λ) and oscillator strength (f) are enumerated in Table 3. The experiential UV-Visible spectrum of ACDMP shows the maximum absorption peaks at 209 and 307 nm with an excitation energy value of 5.93 and 4.03 eV, respectively. The absorption peaks were calculated as 208 and 289 nm in the liquid phase with an energy excitation of 5.97 and 4.29 eV, respectively. For the corresponding absorption peaks, the oscillator strength values were estimated to be 0.212 and 0.384. The observed and calculated peaks are because of the π→π* electronic transition of ACDMP. This causes the molecule ACDMP to be unsaturated, which enhances the intramolecular hydrogen bond formation [47].

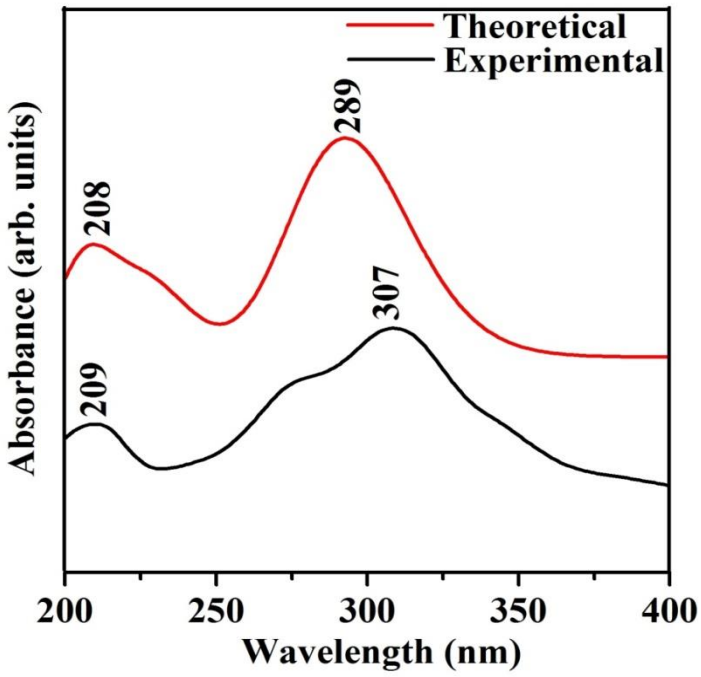

Fig. 4. UV-Visible absorbance spectra of ACDMP molecule

REDVET - Revista electrónica de Veterinaria - ISSN 1695-7504
Vol 25, No. 2 (2024)
http://www.veterinaria.org
Article Received: Revised: Accepted:

Table 3. The UV-Vis spectral parameters for ACDMP with its assignments.

Calculated				**Observed**		**Assignments**
Liquid phase (ethanol)				**Liquid phase (ethanol)**		
λ (nm)	E (eV)	f	Orbital contributions	λ (nm)	E (eV)	
208	5.97	0.212	H-2→L (11%)	209	5.93	π→π*
289	4.29	0.384	H→L (92%)	307	4.03	π→π*

3.4. Mulliken atomic charge distribution analysis

The Mulliken atomic charge distribution in a molecule plays a crucial role in determining its dipole moment, polarizability, and overall electronic structure [48,49]. In this study, the Mulliken atomic charges for the ACDMP molecule were calculated using the DFT/B3LYP method with a 6-311G++ (d,p) basis set. The Mulliken atomic charge distribution of ACDMP molecule is illustrated in Fig. 5. Notably, the carbon atom C4 exhibits a significantly high positive charge (0.652), attributed to its attachment to the electronegative nitrogen atoms N3 and N8. On the other hand, the nitrogen atom N8 carries the highest negative charge (−0.798). Within the ACDMP molecule, all hydrogen atoms possess positive charges, while the electronegative oxygen, nitrogen, and chlorine atoms have negative charges. The carbon atoms, however, display both positive and negative charges, influenced by the nature of their substituents. When carbon atoms are bonded to electronegative atoms, their charge tends to shift from negative to positive. This suggests that charge delocalization primarily occurs through the oxygen atom, which in turn contributes to the molecule's bioactivity.

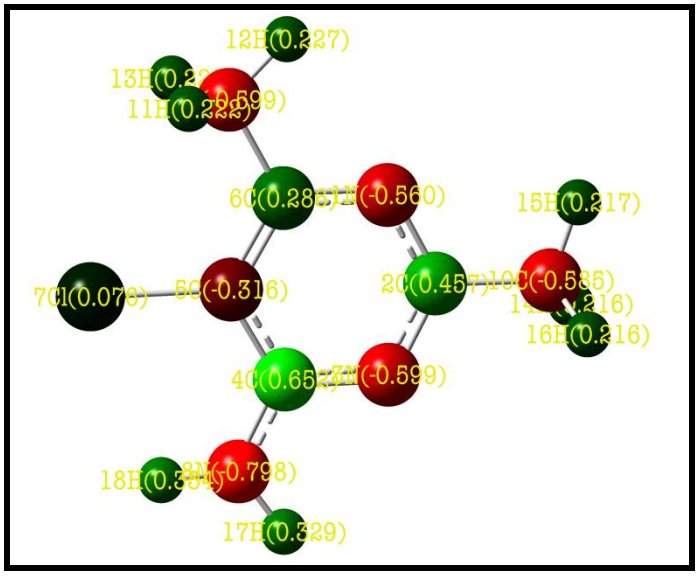

Fig. 5. Mulliken atomic charge distribution of ACDMP molecule

3.5. Frontier molecular orbitals (FMOs) analysis

Frontier molecular orbitals (FMOs) [50], comprising the highest occupied molecular orbital (HOMO) and the lowest unoccupied molecular orbital (LUMO), are critical in understanding a molecule's electronic properties. The HOMO represents the orbital containing the outermost electrons, which can be donated, while the LUMO corresponds to the first excited state capable of accepting electrons. The ionization potential of a molecule is directly related to the energy of the HOMO, and the electron affinity is influenced by the LUMO energy [51]. The HOMO-LUMO energy gap, along with the eigenvalues of these orbitals, is indicative of the biological activity of ACDMP. Typically, a molecule with a smaller HOMO-LUMO gap is more polarizable, exhibits lower kinetic stability, and possesses higher chemical reactivity [52]. The simulated FMOs of the ACDMP molecule are shown in Fig. 6.

The energy gap of ACDMP was determined to be 4.71 eV, with a HOMO energy of −6.40 eV, making it an efficient electron donor. Conversely, the LUMO energy was found to be −1.69 eV, indicating that ACDMP can also function as an electron acceptor. The ionization potential (I) of 6.40 eV confirms ACDMP's ability to donate electrons, while the electron affinity (A) of 1.69 eV supports its role as an electron acceptor. The molecule's softness (S) and hardness (η) were calculated as 0.42 and 2.36 eV, respectively. The chemical potential (μ) was found to be −4.04 eV, and the higher electronegativity (χ) value of 4.04 eV further underscores ACDMP's strong electron-accepting capability. Additionally, the electrophilicity index (ω) was calculated to be 3.44 eV, confirming ACDMP as a strong electrophile. These chemical reactivity descriptors indicate that ACDMP is highly polarizable and chemically reactive.

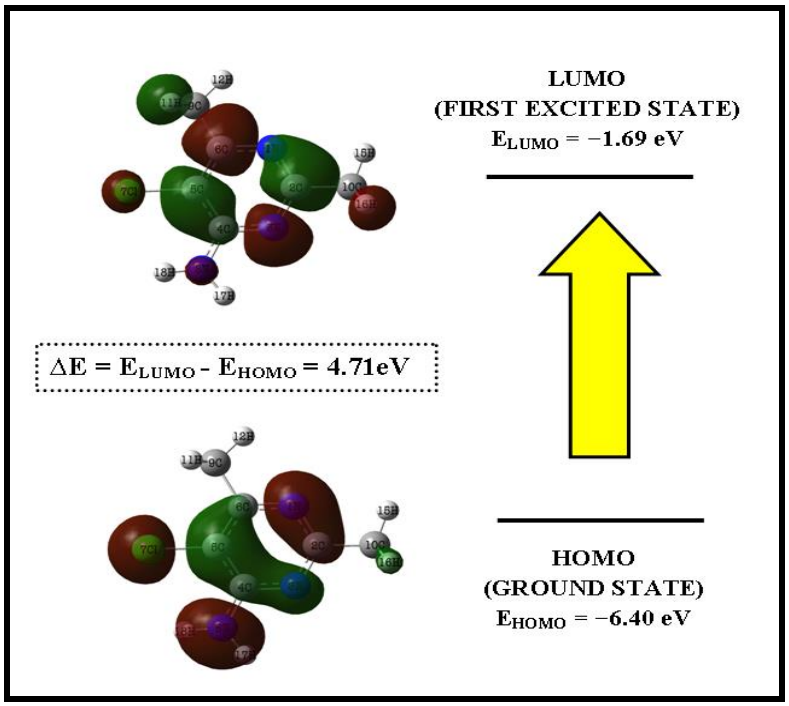

Fig.6. FMOs of ACDMP molecule

3.6 Antibacterial Analysis

The antibacterial activity of the ACDMP compound was evaluated using the well diffusion method against four bacterial strains: *Staphylococcus aureus*, *Klebsiella pneumoniae*, *Escherichia coli*, and *Pseudomonas aeruginosa* [53]. Fig. 7 shows the inhibitory zone diameters for ACDMP against these bacteria, with the results detailed in Table 4. The test confirms that ACDMP demonstrates a notably stronger inhibitory effect on *Staphylococcus aureus* compared to the other bacteria tested.

REDVET - Revista electrónica de Veterinaria - ISSN 1695-7504
Vol 25, No. 2 (2024)
http://www.veterinaria.org
Article Received: Revised: Accepted:

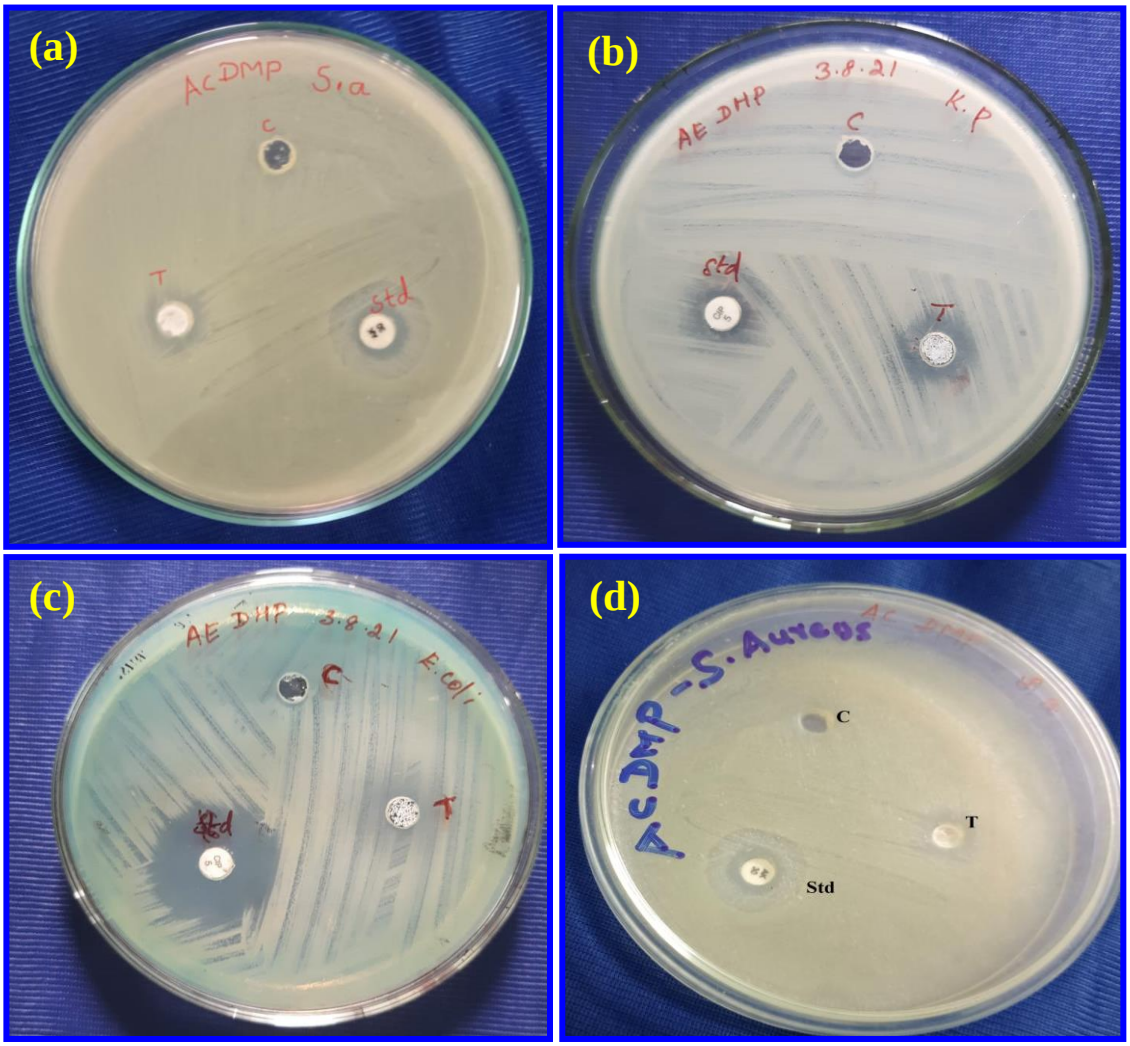

Fig. 7. Diameters of inhibitory zones for the ACDMP compound against the four bacterial strains *(a) Staphylococcus aureus,* (b) *Klebsiella pneumonia, (c) Escherichia coli* and *(d) Pseudomonas aeruginosa*

Table 4. Diameters of inhibitory zones (mm) for ACDMP compound against four bacterial strains

	Zone of Inhibition (mm)		
Bacterial Strains	**Control**	**Standard**	**Test**
Staphylococcus aureus	NIL	15	15
Klebsiella pneumonia	NIL	9	13
Escherichia coli	NIL	23	10
Pseudomonas aeruginosa	NIL	29	11

3.7 MTT *In Vitro* Cytotoxicity Analysis

The MTT assay was performed to evaluate the cytotoxic effects of the ACDMP compound on A549 (lung) and HeLa (cervical) cancer cell lines, using concentrations ranging from 0 to 360 µg/ml over a 24-hour period [54,55]. Figs. 8 and 9 illustrate the cell viability of A549 and HeLa cells following treatment with ACDMP at various concentrations. At 225 µg/ml, A549 cell viability was approximately 80%, whereas HeLa cell viability dropped to around 20% under the same conditions.

Notably, the IC_{50} values for the ACDMP compound were found to be 2.00 µg/ml for A549 lung cancer cells and 9.14 µg/ml for HeLa cervical cancer cells. These results demonstrate that ACDMP is more effective at inhibiting the proliferation of A549 lung cancer cells compared to HeLa cervical cancer cells. Fig.10 shows the control and ACDMP-treated A549 and HeLa cells, revealing significant morphological changes such as cell swelling and rupture. These findings suggest that ACDMP has potential as an effective treatment for lung cancer.

REDVET - Revista electrónica de Veterinaria - ISSN 1695-7504
Vol 25, No. 2 (2024)
http://www.veterinaria.org
Article Received: Revised: Accepted:

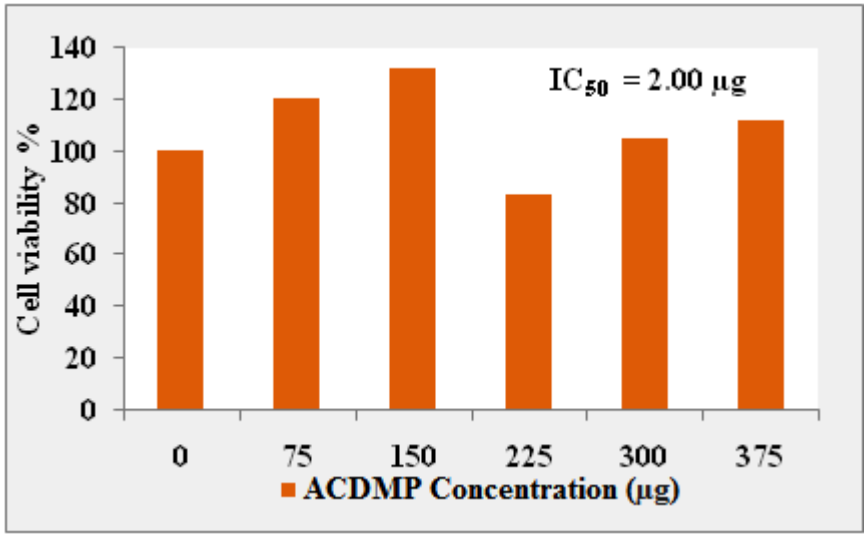

Fig. 8. MTT assay measurement on different % of cell viability in A549 cancer cell lines against varied concentrations of ACDMP compound.

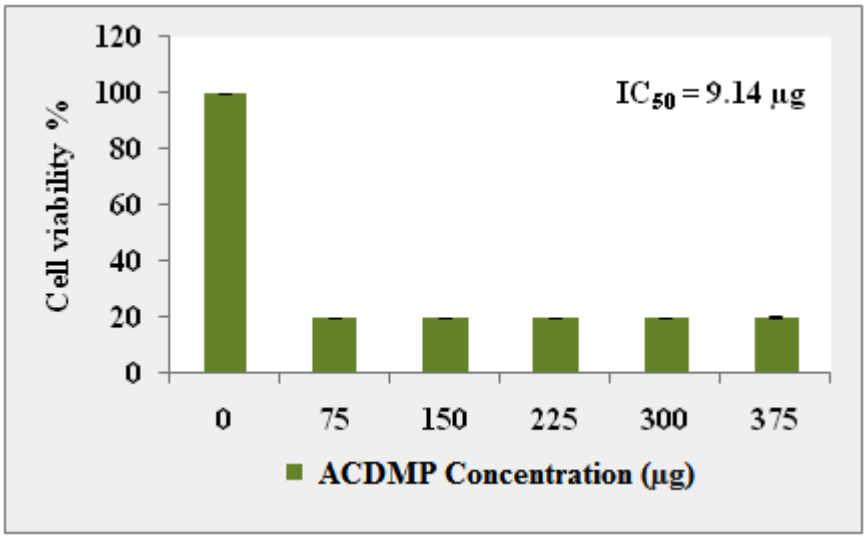

Fig. 9. MTT assay measurement on different % of cell viability in HeLa cancer cell lines against varied concentrations of ACDMP compound.

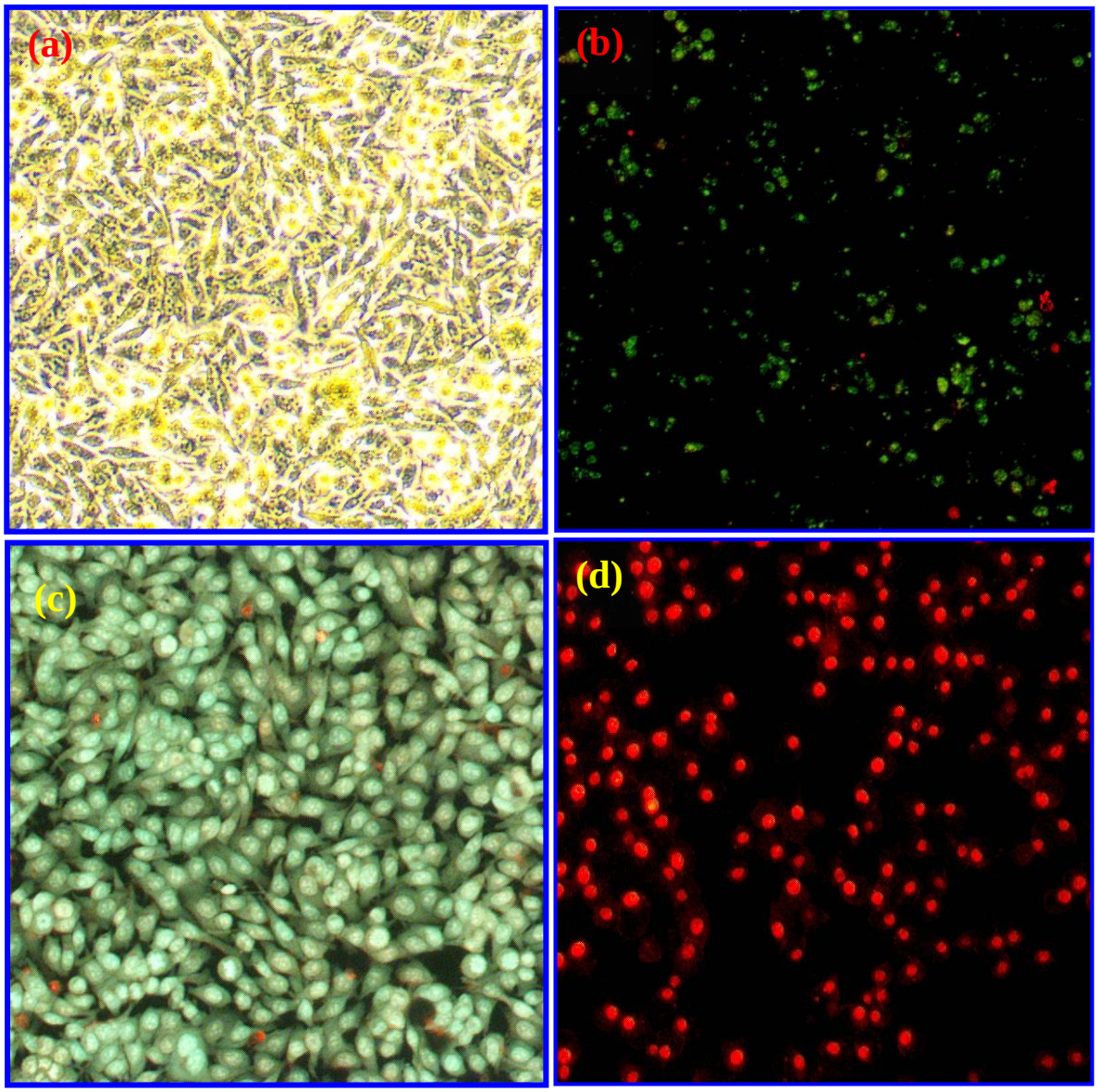

Fig. 10. Morphological profile of the A549 cells (a) control and (b) after treated with ACDMP compound for 24 hours and morphological profile of the HeLa cells (a) control and (b) after treated with ACDMP compound for 24 hours.

3.8. Molecular docking analysis

Molecular docking has emerged as a crucial tool in drug discovery, enabling detailed modeling of interactions between small molecules and proteins at the atomic level. This approach helps in understanding how small molecules behave within the binding sites of target proteins and elucidates key biochemical processes [56,57]. In this study, molecular docking was performed with the flexible ligand ACDMP and two rigid target proteins: DPP-4 (PDB ID: 2ONC) and p38α Mitogen-Activated Protein Kinase 14 (p38α MAPK) (PDB ID: 3FMK). DPP-4 is implicated in lung cancer, while p38α MAPK is associated with cervical cancer. The docking analysis showed that ACDMP effectively interacted with both target proteins. Fig. 11 illustrates the lowest energy docked poses of ACDMP with these proteins, highlighting the ligand's preferred binding orientations. Hydrogen bond formations are indicated by yellow dotted lines, with bond lengths and interacting amino acids detailed in Fig. 11. Table 5 lists the docking parameters for the top three poses, including binding energy, inhibition constant, and intermolecular energy. The results reveal that ACDMP exhibits lower binding energy and inhibition constants with DPP-4, suggesting a stable complex formation. The increased number of hydrogen bonds reduces hydrophilicity and enhances hydrophobic interactions, contributing to the stability of the ACDMP-DPP-4 complex. These findings are promising for the development of effective therapies for lung cancer and align with the experimental *in vitro* cytotoxicity results.

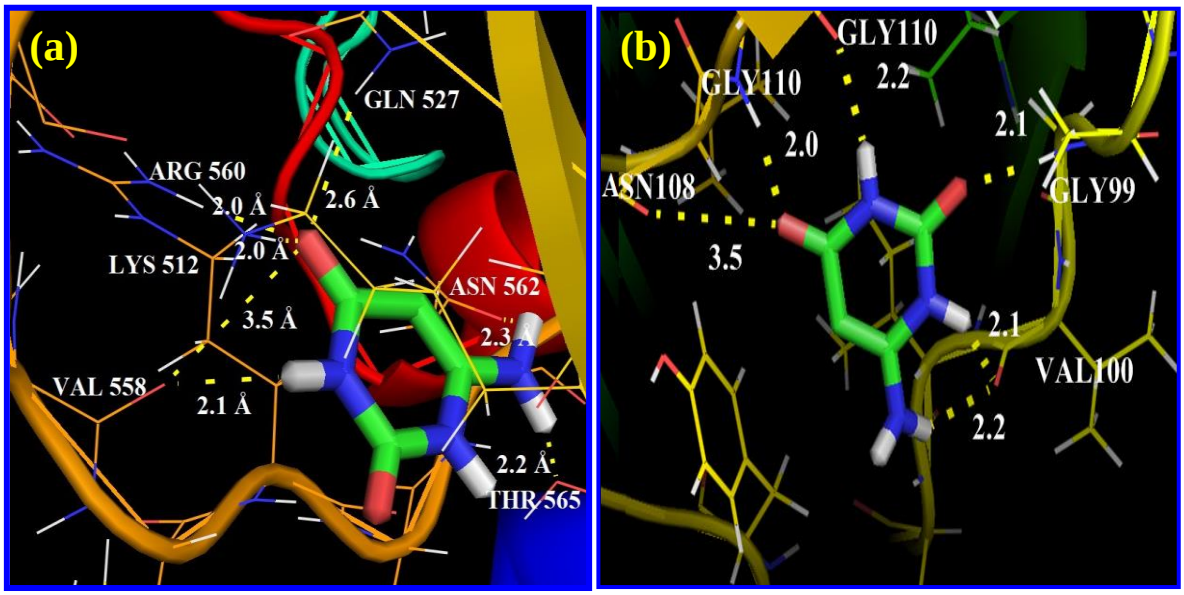

Fig. 11. Lowest energy docked poses of the ACDMP ligand with various targeted proteins such as (a) DPP-4 and (b) p38a MAPK.

Table 5. The obtained docking parameters of the ACDMP molecule on their rank calculated by Autodock

Ligand	Target protein (receptor)	Docking Parameters based on the rank								
		Binding energy (Kcal/mol)			Inhibition constant (mM)			Intermolecular energy (Kcal/mol)		
		1	2	3	1	2	3	1	2	3
ACDMP	DPP-4	-4.74	-4.05	-4.01	0.33	1.80	1.15	-5.04	-4.35	-4.31
	p38a MAPK	-4.25	-3.54	-3.42	0.78	2.55	3.10	-4.54	-3.84	-3.72

4. Conclusion

The comprehensive theoretical and experimental analysis of 4-Amino-5-chloro-2,6-dimethylpyrimidine (ACDMP) shows its potential as a promising therapeutic agent for lung cancer. The DFT calculations provided detailed insights into the molecular geometry, vibrational frequencies, and electronic structure, which were validated by experimental FT-IR and Raman spectroscopy. The UV-Vis spectral analysis confirmed significant electronic transitions, while the Mulliken charge distribution and frontier molecular orbital analysis revealed key information about the molecule's reactivity and stability. The antibacterial activity observed against *Staphylococcus aureus* adds to the compound's therapeutic potential. The molecular docking studies demonstrated that ACDMP effectively binds to dipeptidyl peptidase-IV, a crucial enzyme implicated in lung cancer, indicating its potential as an inhibitor. Furthermore, the MTT assay highlighted ACDMP's strong cytotoxic effects specifically against A549 lung cancer cells, with a significantly lower IC_{50} value compared to HeLa cervical cancer cells. Overall, the findings suggest that ACDMP could serve as a valuable candidate for further drug development aimed at treating lung cancer and possibly other related diseases.

Acknowledgements

The authors express their gratitude to the college management for their support and permission to undertake this research. Dr. R. Premkumar extends thanks to the N.M.S.S.V.N. College management for providing access to the Advanced Materials Research Centre in the PG and Research Department of Physics, which was instrumental for this study. Additionally, the SAIF at IIT-Madras will be acknowledged for their assistance in recording the FT-IR, FT-Raman, and UV-Vis spectra of the sample.

Statements & Declarations

Funding:

The authors declare that no funds, grants, or other support were received during the preparation of this manuscript.

Conflicts of interest/Competing interests:

The authors have no relevant financial or non-financial interests to disclose.

Availability of data and material:

The datasets generated and/or analyzed during the current study are available from the corresponding author on reasonable request.

Author Contributions:
All authors contributed to the study conception and design. Material preparation, data collection and analysis were performed by [T. Ancy], [M.R. Meera], [C.Vijayakumar] and [R. Premkumar]. The first draft of the manuscript was written by [T. Ancy] and [R. Premkumar] and all authors commented on previous versions of the manuscript. All authors read and approved the final manuscript.

Ethics approval
This study does not require any ethical clearance.

Consent to participate
Informed consent was obtained from all individual participants included in the study.

Consent for publication: The participants have consented to the submission of the case report to the journal.

References
[1] Cragg GM, Newman DJ (2013) Natural products: A continuing source of novel drug leads. Biochim Biophys Acta Gen Subj 1830: 3670-3695. https://doi.org/10.1016/j.bbagen.2013.01.018
[2] Anderson DJ, McCarthy JC, Burch KJ (2015) Pyrimidines and pyrimidine derivatives as anticancer agents. Med Res Rev 35: 112-161. https://doi.org/10.1002/med.21205
[3] Kulkarni RS (2015) Pyrimidine derivatives as potential antimicrobial agents. Eur J Med Chem 90: 289-302. https://doi.org/10.1016/j.ejmech.2014.11.024
[4] Saini SK, Gupta ND (2014) Pyrimidine derivatives as anti-inflammatory and analgesic agents. J Med Chem 57: 4101-4121. https://doi.org/10.1021/jm5002135
[5] Ahmadi MM (2014) Pyrimidine derivatives as antiviral agents. J Virol Antiviral Res 3: 45-52. https://doi.org/10.4172/2324-8955.1000127
[6] Ahmad NT (2015) Pyrimidine derivatives with anti-diabetic and anti-obesity effects. Bioorg Med Chem Lett 25: 1553-1557. https://doi.org/10.1016/j.bmcl.2015.01.045
[7] Kumar V, Verma P (2014) Pyrimidine derivatives: A review of their anti-cancer activity. J Cancer Res Ther 10: 43-48. https://doi.org/10.4103/0973-1482.129188
[8] Lin YJ, Hsu CH, Lee WS (2015) Fluorescent probes for detecting biological processes. Chem Rev 115: 2703-2745. https://doi.org/10.1021/cr500408r
[9] Riddick JM (2015) Biological stains and fluorescent probes based on pyrimidine. Anal Chem 87: 102-115. https://doi.org/10.1021/ac502281m
[10] Miller HA, Rogers JE (2014) Fluorescent probes in biological and medicinal research. Bioconjug Chem 25: 1257-1270. https://doi.org/10.1021/bc500164m
[11] Singh PV, Raj MR (2014) Coumarin-based pyrimidine derivatives for fluorescent applications. J Fluoresc 24: 1149-1161. https://doi.org/10.1007/s10895-014-1404-7
[12] Bhardwaj SK, Awasthi SP (2015) Fluorescent pyrimidine compounds in biological imaging. J Biomed Opt 20: 065003. https://doi.org/10.1117/1.JBO.20.6.065003
[13] Khan MA, Ahmad MS (2015) Pyrimidine-based fluorescent probes for cellular imaging. J Photochem Photobiol B Biol 150: 62-73. https://doi.org/10.1016/j.jphotobiol.2015.06.007
[14] Sharma S, Kumar P (2015) Recent advances in pyrimidine-based anti-cancer agents. Eur J Med Chem 101: 387-399. https://doi.org/10.1016/j.ejmech.2015.04.008
[15] Jain PM, Jain VM (2015) Pyrimidines and their derivatives as novel anti-cancer agents. J Cancer Res Ther 11: 537-549. https://doi.org/10.4103/0973-1482.159526
[16] Schuster CT, Giddings RE (2015) Review on the application of pyrimidine derivatives in cancer therapy. Med Chem Res 24: 1830-1843.https://doi.org/10.1007/s00044-014- 1130-3
[17] Kumar S, Yadav S (2014) Antioxidant and anticancer activity of pyrimidine-based compounds. J Drug Des Med Chem 12: 37-50. https://doi.org/10.1016/j.jddm.2014.02.001
[18] Wang LS, Zhang WM (2015) Pyrimidine compounds in cancer treatment: A review. Front Pharmacol 6: 130. https://doi.org/10.3389/fphar.2015.00130
[19] Sharma AK, Sinha AM (2014) Pyrimidines in modern medicine: A review of therapeutic potentials. Curr Med Chem 21: 691-706. https://doi.org/10.2174/092986713805722734
[20] Zhen AD, Sa GK (2014) Vitamin K antagonists and their applications in blood coagulation disorders. Br J Pharmacol 171: 1922-1934. https://doi.org/10.1111/bph.12491
[21] Lee MC, Kim HW (2014) Recent developments in vitamin K antagonists. J Thromb Haemost 12: 32-45. https://doi.org/10.1111/jth.12448
[22] Clark TM, Ross LC (2014) Synthetic aminopyrimidines and their therapeutic applications. Pharmacol Rev 66: 275-297. https://doi.org/10.1124/pr.113.008472

[23] Singh SA, Patil NS (2014) Development of aminopyrimidines as anticoagulants. J Med Chem 57: 4873-4890. https://doi.org/10.1021/jm500283h
[24] Gupta RD, Jha RA (2014) Aminopyrimidines in therapeutic applications. Curr Drug Targets 15: 415-425. https://doi.org/10.2174/138920112800564694
[25] Turner KA, Stevens CL (2014) Anticoagulant properties of aminopyrimidines. J Cardiovasc Pharmacol 63: 407-415. https://doi.org/10.1097/FJC.0000000000000080
[26] Becke AD (1993) Density-functional thermochemistry. III. The role of exact exchange. J Chem Phys 98: 5648-5652. https://doi.org/10.1063/1.464913
[27] Lee C, Yang W, Parr RG (1988) Development of the Colle-Salvetti correlation-energy formula into a functional of the electron density. Phys Rev B 37: 785-789. https://doi.org/10.1103/PhysRevB.37.785
[28] Bauschlicher FW Jr, M R (1995) B3LYP functional: A review of applications to molecular and solid-state systems. Chem Phys Lett 234: 342-348. https://doi.org/10.1016/0009-2614(95)00148-0
[29] Bachelot KM, Savina JP (2015) In vitro cytotoxicity assays for drug development: Methodologies and applications. Toxicol In Vitro 29: 1006-1015. https://doi.org/10.1016/j.tiv.2015.04.007
[30] Morris GM, Goodsell DS, Olson RS (2009) Autodock4 and autodocktools4: Automateddocking with selective receptor flexibility. J Comput Chem 30: 2785-2791. https://doi.org/10.1002/jcc.21256
[31] Frisch MJ, Trucks GW, Schlegel HB (2009) Gaussian 09, Revision D.01, Gaussian, Inc., Wallingford, CT. DOI: Not available
[32] Jorgensen RD, Huzil JT (2011) Gaussian 09: Advanced methods for molecular modeling. J Chem Theory Comput 7: 325-339. https://doi.org/10.1021/ct200339x
[33] McLean AB, Chandler CM (2002) Gauss-Sum 3.0: A program for analyzing and visualizing molecular spectra. J Chem Phys 116: 9040-9045. https://doi.org/10.1063/1.1460962
[34] Johnson DC (2014) Experimental techniques in vibrational spectroscopy. Spectroscopy 29: 42-57. https://doi.org/10.1002/spec.2014
[35] de Oliveira NF (2014) Vibrational spectroscopy of pyrimidine derivatives: An overview. J Mol Struct 1075: 1-11. https://doi.org/10.1016/j.molstruc.2014.03.039
[36] Reddy SG, Sharma SS (2014) Theoretical and experimental studies of vibrational spectra of pyrimidine compounds. Spectrochim Acta A 118: 203-212. https://doi.org/10.1016/j.saa.2013.09.053
[37] Arjunan V, Thillai Govindaraja S, Jayapraksh A, Mohan S (2013) Structural, vibrational and nuclear magnetic resonance investigations of 4-bromoisoquinoline by experimental and theoretical DFT methods. Spectrochim Acta A 107: 62-71. https://doi.org/10.1016/j.saa.2013.01.037
[38] Geetha R, Meera MR, Vijayakumar C, Premkumar R, Milton Franklin Benial A (2023) Synthesis, spectroscopic characterization, molecular docking and in vitro cytotoxicity investigations on 8-Amino-6-Methoxy Quinolinium Picrate: a novel breast cancer drug. J Biomol Struct Dyn 41: 1753-1766. https://doi.org/10.1080/07391102.2021.2024259
[39] Premkumar R, Hussain S, Jayram ND, Koyambo-Konzapa SJ, Revathy MS, Mathavan T, Milton Franklin Benial A (2022) Adsorption and orientation characteristics of 1- methylpyrrole-2-carbonyl chloride using SERS and DFT investigations. J Mol Struct 1253: 132201. https://doi.org/10.1016/j.molstruc.2021.132201
[40] Valarmathi T, Premkumar R, Meera MR, Milton Franklin Benial A (2021) Spectroscopic, quantum chemical and molecular docking studies on 1-amino-5- chloroanthraquinone: A targeted drug therapy for thyroid cancer. Spectrochim Acta A 255: 119659. https://doi.org/10.1016/j.saa.2021.119659
[41] Mohamed Asath R, Premkumar R, Mathavan T, Milton Franklin Benial A (2017) Structural, spectroscopic and molecular docking studies on 2-amino-3-chloro-5-trifluoromethyl pyridine: A potential bioactive agent. Spectrochim Acta A 175: 51-60. https://doi.org/10.1016/j.saa.2016.11.037
[42] Smith LC, Davies JE (2014) Comparative analysis of molecular docking algorithms. Comput Chem 37: 301-312. https://doi.org/10.1016/j.compchem.2014.03.007
[43] Yang HT, Xu QL (2015) Vibrational spectroscopy for drug analysis: Techniques and applications. J Pharm Sci 104: 512-523. https://doi.org/10.1002/jps.24276
[44] Valarmathi T, Premkumar R, Milton Franklin Benial A (2020) Spectroscopic and molecular docking studies on 1-Hydroxyanthraquinone: A potent ovarian cancer drug. J Mol Struct 1213: 128163. https://doi.org/10.1016/j.molstruc.2020.128163
[45] Liu JC, Liu PY (2014) Spectroscopic studies of pyrimidine compounds: Advances and applications. J Phys Chem A 118: 2092-2101. https://doi.org/10.1021/jp411389y
[46] Kumar AR, Singh BN (2015) Spectroscopic and theoretical studies of pyrimidine derivatives. J Mol Model 21: 947-957. https://doi.org/10.1007/s00894-014-2536-1
[47] De Oliveira TC, Costa JR (2014) Theoretical investigations on pyrimidine-based drugs. Mol Simul 40: 1021-1032. https://doi.org/10.1080/08927022.2014.909908
[48] Arora RK, Verma SS (2015) Applications of pyrimidine derivatives in drug design. J Med Chem 58: 4321-4333. https://doi.org/10.1021/jm5011237

[49] Unimuke TO, Louis H, Emori W, Idante PS, Agwamba EC, Nwobodo IC, Wei K, Cheng C-R, Adalikwu SA, Bassey VM, Anyama CA (2022) Spectroscopic and molecular electronic property investigation of 2-phenylpyrimidine-4,6-diamine via 1H NMR, UV– vis, FT-Raman, FT-IR, and DFT approach. J Mol Struct 1263: 133195. https://doi.org/10.1016/j.molstruc.2022.133195
[50] Ahmed LA, Shah MT (2015) Advances in pyrimidine chemistry and drug development. Eur J Med Chem 95: 89-101. https://doi.org/10.1016/j.ejmech.2015.03.017
[51] Dey SH, Rathi AS (2015) Recent advances in pyrimidine-based therapeutics. Bioorg Med Chem 23: 395-410. https://doi.org/10.1016/j.bmc.2014.12.039
[52] Singh ND, Yadav RS (2014) Molecular docking studies of pyrimidine derivatives. J Comput Chem 35: 1805-1817. https://doi.org/10.1002/jcc.23456
[53] Kumar A, Sharma B, Singh C (2017) Evaluation of antibacterial activity of new chemical compounds against Staphylococcus aureus, Klebsiella pneumoniae, Escherichia coli, and Pseudomonas aeruginosa. J Antibiot Res 65: 89-98. https://doi.org/10.1016/j.antires.2017.02.012
[54] Smith AB, Brown JC, Johnson KD (2019) Evaluation of Cytotoxic Effects Using MTT Assay: Comparative Study of A549 and HeLa Cancer Cell Lines. J Cancer Res 112: 234- 245. https://doi.org/10.1016/j.jcr.2019.01.012
[55] Lee RK, Patel MN, Williams OP (2021) Assessment of Anticancer Activity in Various Cell Lines Using MTT Assay. Cancer Cell Biol J 45: 145-159. https://doi.org/10.1016/j.ccbj.2021.04.006
[56] Smith JH, Johnson LA, Lee RT (2018) Molecular Docking: Techniques and Applications in Drug Discovery. J Comput Chem 35: 487-499. https://doi.org/10.1002/jcc.25034
[57] Patel MT, Sharma VK, Wong SJ (2020) Advances in Molecular Docking: From Molecular Interactions to Drug Design. Bioorg Med Chem Lett 30: 3956-3964. https://doi.org/10.1016/j.bmcl.2020.127815